MHD IN VON KÁRMÁN SWIRLING FLOWS

development and first run of the VKS experiment

L. MARIÉ, J. BURGUETE, A. CHIFFAUDEL*, F. DAVIAUD, D. ERICHER, C. GASQUET
DSM/DRECAM/SPEC, CEA/Saclay, (*) C.N.R.S.
91191 Gif sur Yvette cedex, France

F. PETRELIS, S. FAUVE
École Normale Supérieure
25, rue Lhomond, F-75005, France

M. BOURGOIN, M. MOULIN, P. ODIER, J.-F. PINTON
École Normale Supérieure de Lyon, CNRS
46, allée d'Italie, F-69364 Lyon, France

A. GUIGON, J.-B. LUCIANI, F. NAMER
DRN/DER/STPI, CEA/Cadarache
13108 Saint Paul les Durance, France

AND

J. LÉORAT
Observatoire de Paris-Meudon
92195 Meudon, France

1. Introduction

1.1. MOTIVATION

The magnetism of many astrophysical objects, such as various stars or planets, galaxies, the intergalactic medium, etc, is attributed to the motion of conducting fluid in their interiors. It has been first proposed by Larmor (Larmor, 1919) that a flow of conducting fluid generates the magnetic field of the sun by maintaining the corresponding electric current against ohmic dissipation. Such a generation of electromagnetic energy from mechanical work using a self-excited dynamo has been known since Siemens (Roberts and Jensen, 1993) and is the most basic mechanism of electrical engineering. However, in industrial dynamos the path of the electric currents are constrained by a complex wiring, which even in the most

elementary device, the homopolar dynamo (Bullard, 55), breaks mirror symmetry. In addition, magnetic field lines are usually canalized using a high magnetic permeability material. No such well controlled external constraints on the field or on the current lines exist in "natural" dynamos, and for a long time, it has been far from obvious that the dynamo effect was the correct explanation for solar or earth magnetism. It has been even shown that a lot of flow and / or field configurations with enough symmetries cannot behave as fluid dynamos [for a review on anti-dynamo theorems, see Kaiser et al., these proceedings].

The first simple example of an homogeneous dynamo (i. e. in a medium of constant electrical conductivity and thus no path of least resistance) was given by Herzenberg (Herzenberg, 1958). It consists of 2 or 3 rotating solid spheres embedded in a static medium of the same conductivity with which they are in perfect electrical contact. A slightly different version of the Herzenberg dynamo was operated experimentally by Lowes and Wilkinson and may be considered as the first experimental demonstration of a homogeneous dynamo (Lowes and Wilkinson, 1993). In a simply connected domain, the simplest "flow" leading to dynamo action was found by Ponomarenko (Ponomarenko, 1972). It consists of a cylinder in solid body rotation and translation along its axis, embedded in an infinite static medium of the same conductivity with which it is in perfect electrical contact. Each point of the cylinder thus follows an helical path. Another simple flow has been found by G. O. Roberts (G.O. Roberts, 1972). It is a spatially periodic flow that consists of a two-dimensional array of helical eddies. It should be noted that the three velocity fields, $\vec{v}$, quoted above, have a non zero helicity $\langle \vec{v} \cdot \vec{\nabla} \times \vec{v} \rangle$, where $\langle \cdot \rangle$ stands for the spatial average. Although this is not a necessary condition for dynamo action, it has been shown by Parker that the non zero helicity of cyclonic eddies leads to an efficient dynamo mechanism (Parker, 1955).

Very recent experiments using a Ponomarenko type [the Riga experiment (Galaitis *et al.*, 2000a; Galaitis *et al.*, 2000b), these proceedings] or a Roberts type [the Karlsruhe experiment (Stieglitz *et al.*, 2000), these proceedings] flow of liquid sodium, have provided the first laboratory models of fluid dynamos. However, an experimental demonstration of the dynamo effect in an unconstrained turbulent flow of liquid metal is still lacking. This is the main objective of our experiments using von Kármán swirling flows of liquid gallium and sodium. The possibility of generating a dynamo action in a flow whose large scale velocity field comes close to the geometries considered by Dudley and James (Dudley and James, 1989) has been suggested by Roberts and Jensen (Roberts and Jensen, 1993). This has led to experiments where the fluid is confined in a closed tank and the flow is produced by the motion of 'stirrers'. One such experiment is being run by

the Maryland group and has yielded results on MHD turbulence (Peffley *et al.*, 2000)[Maryland group, these proceedings]. Another is planned by the group in Madison [the Madison experiment, these proceedings]. Our motivations for studying the dynamo in the von Kármán geometry are the following ones:

1) Effect of turbulence on the dynamo onset

In the absence of strong geometrical constraints, any flow of liquid metal is fully turbulent before possibly displaying dynamo action. Indeed, the magnetic Prandtl number, $Pm = \mu_0 \sigma \nu$, where μ_0 is the magnetic permeability of vacuum, σ is the electric conductivity of the fluid and ν is its kinematic viscosity, is smaller than 10^{-5} for all electrically conducting liquids. Since the dynamo action requires a large enough magnetic Reynolds number, $Rm = \mu_0 \sigma L V$, where V is the fluid characteristic velocity and L is the flow characteristic large scale, one expects to observe the dynamo effect when the flow kinetic Reynolds number, $Re = VL/\nu$, is larger than 10^6. The role of turbulent fluctuations at such large Reynolds numbers may be twofold: on one hand, they decrease the effective electrical conductivity and thus inhibits dynamo action by increasing Joule dissipation. On the other hand, they may generate a large scale magnetic field through the "alpha effect" or higher order similar effects (Krause and Rädler, 1955; Moffatt, 1978). Experiments are the only way to study the role of turbulent fluctuations because direct numerical simulations cannot be performed at such high Reynolds number.

2) Saturation of the magnetic field

The saturation mechanisms of the growth of the magnetic field above the dynamo onset should strongly depend on the geometrical constraints applied to the flow. Indeed, an unconstrained flow is more easily perturbed under the action of the Lorentz force and this is likely to affect the post-bifurcation regime. A problem of fundamental interest is to determine the mean magnetic energy and the mean Joule dissipation related to their kinetic counterparts in the supercritical saturated regime. Again, this can be studied only experimentally because direct simulations of the dynamical dynamo problem with realistic values of the magnetic Prandtl number cannot be performed.

3) Dynamical and statistical properties of the generated magnetic field

Magnetic fields of astrophysical objects may be found to be almost time-periodic, like in the sun, or nearly stationary i. e. very slowly varying, like for the earth magnetic field between two successive reversals. It is tempting to connect this temporal behavior with the nature of the dynamo bifurcation which can be either a stationary bifurcation or a Hopf bifurcation in the simplest generic cases. It should be noted that both a stationary bifurcation (Karlsruhe experiment), and a Hopf bifurcation (Riga experiment) have

been observed so far. With these simple geometry flows, it is possible to guess the nature of the bifurcation using symmetry considerations. This is less obvious in the case of a fully developed turbulent flow and it would be interesting to try to understand how is determined the dynamical regime above the dynamo onset. Another interesting question with flows involving relative turbulent fluctuations as large as 50%, is to determine whether the dynamo is generated mostly from the mean flow or predominantly from the turbulent fluctuations. Finally, the study of the statistical properties of magnetohydrodynamic turbulence without an externally applied field, and the observation of the dynamics of the large scale magnetic field (reversals) are of fundamental interest and may also improve our understanding of solar or terrestrial magnetism.

1.2. WHY THE VON KÁRMÁN FLOW GEOMETRY ?

The choice of an optimum configuration to perform a turbulent dynamo experiment is not an easy task. As said above, if the flow is not confined by internal boundaries, it is strongly turbulent when the dynamo action may occur. In the case of confined flows, turbulent fluctuations are of course also generated at large Reynolds numbers, but they are restricted to small scales. The large eddies that generate the magnetic field in the Karlsruhe (Stieglitz *et al.*, 2000) or Riga (Galaitis *et al.*, 2000a; Galaitis *et al.*, 2000b) experiments are quenched by the internal boundaries and thus forced to act coherently in time. This is not the case for unconfined flows in which the large scale flow may have undergone several bifurcations before the dynamo onset. Thus, both the geometry of the large eddies as well as their time dependence are difficult to predict. Since direct numerical simulations are not possible at kinetic Reynolds numbers of order 10^6, the efficiency of a given set-up with respect to dynamo action cannot be even roughly evaluated before having characterised the flow using water experiments. However, there are general arguments that have motivated our choice of von Kármán type flows. We will first shortly describe these flows and then discuss the motivations which have led us to use them in a dynamo experiment.

Flows that are generated between two co-axial rotating discs (see figure 1 and 4) have been called "von Kármán swirling flows" (Zandenbergen and Dijkstra, 1987). Mean velocity profiles in cases where the flow is confined inside cylindrical walls have been measured since the late fifties (Picha, 1957; Picha and Eckert, 1958; Welsh, 1958; Simand *et al.*, 2000; Burguete *et al.*, 2000). In the case of co-rotating discs, one observes that the flow can be split into two parts: (i) a central core, nearly in solid body rotation at an average angular speed, the radius of which is fixed by the distance

between the discs; (ii) an external flow driven outward near the discs by the centrifugal forces, and consequently, inward in the mid-plane. At high Reynolds numbers the whole flow is turbulent.

Kármán swirling flows generated with counter-rotating discs strongly differ from the co-rotating case: a time average of the velocity field (see figure 1) shows the existence of differential rotation and meridian recirculation loops. No coherent stationary average flow can be observed, although slowly drifting coherent structures have been detected in the median region (Daviaud *et al.*, 2000). In the central region, a well defined average motion is not observed and large and random turbulent velocity fluctuations occur (Picha and Eckert, 1958; Pinton and Labbé, 1994; Mordant *et al.*, 1997). Visualisation using water seeded with air bubbles, shows intermittent formation of filaments of bubbles that are ascribed to vorticity concentrated on tube-like structures (Douady *et al.*, 1991; Fauve *et al.*, 1993; Cadot *et al.*, 1995; Dernoncourt *et al.*, 1998).

The first motivation to try a dynamo experiment using von Kármán flows relied on their efficiency to amplify and concentrate vorticity. Pressure measurements showed that localized vortex involves velocity increments on their core size of the order of the integral velocity (Fauve *et al.*, 1993) and it has been further shown that the typical core size is of the order of the flow Taylor microscale (Dernoncourt *et al.*, 1998). Although we know that the Elsasser analogy between vorticity and magnetic field cannot be used without caution, a flow which is an efficient amplifier of vorticity is likely to be a good candidate for a dynamo experiment.

A second argument is the existence of local helicity in the vicinity of the rotating discs that generate strong swirling flows of identical helicity (respectively opposite) in the contra-rotating case (respectively co-rotating). Although not necessary, the existence of helicity or the weaker condition of the absence of mirror symmetry, are known to be in favor of dynamo action.

Finally the amount of turbulent fluctuations with respect to the mean flow can be easily modified in the von Kármán geometry. Turbulent fluctuations are much larger in the counter-rotating case and it is also easy to get a time dependent large scale mean flow by rotating the two discs at different angular velocities (Simand *et al.*, 2000). These aspects are obviously interesting in order to study the effect of turbulent fluctuations on the dynamo onset. Indeed, the mean flow has been measured and the threshold of dynamo action resulting from the mean flow alone has been computed using a kinematic code (Burguete *et al.*, 2000) [section 2, below].

There are of course other well-known turbulent flows in closed geometries that may be considered. Thermal convection is certainly of interest in

astrophysical or geophysical contexts but it is probably a very inefficient way to get a dynamo on the laboratory scale. Flows generated by inertial forces may fall in the same category (Malkus, 1968). If one is interested by scale separation between the velocity field and the magnetic field, Couette-Taylor flow may be tried as a possible way to achieve such a configuration without internal boundaries (Laure *et al.*, 2000).

2. Optimization

Self-excitation is expected if the magnetic Reynolds number Rm exceeds a critical value Rm^c. In order for this to be achieved experimentally, one must optimize the flow configuration to have the lowest possible threshold and maximize the range of accessible Rm in the set-up. The latter is fixed by the amount of mechanical power P input into the flow: due to the low magnetic Prandtl number Pm of all liquid metals, even moderate Rm flows are strongly turbulent. As a result, given the characteristic length scale L of the flow, P scales as $P \sim \rho L^2 U^3$, so that $Rm^{\max} \sim \mu\sigma(PL/\rho)^{1/3}$, and is thus weakly influenced by size or power. Much stronger variations result from the flow geometry. Given the choice of the von Kármán flow class, one optimizes the entrainment device (poloidal vs. toroidal velocities) and boundary conditions (insulating or conducting outer shell). The main characteristics of the velocity field are measured for various discs drives and configurations in a water experiment and then introduced in a kinematic dynamo computer simulation. The water setup is a half-scale model, in a cylindrical ($R = 10$ cm) vessel – at 50°C, the viscosity of water is closed to that of sodium at 120°C. Both global (power consumption) and local velocity measurements are made. Power is measured via torque and global temperature increase measurements. For large kinetic Reynolds numbers, the results exhibit a variation of the power as $P \sim \Omega^3$, with Ω the rotation frequency, in agreement with scaling predictions. The mean velocity field is obtained via Laser Doppler Anemometry and pulsed Doppler Ultrasonic Velocimetry – typical results are shown in figure 1. The local rms velocity fluctuations (relative to the mean) give a typical turbulence rate of 50 %.

A kinematic dynamo code is developed in a periodic cylindrical domain, with a pseudospectral scheme in the azimuthal and axial directions and finite differences in the radial direction (Léorat, 1999). The conductivity of fluid σ inside the cylinder is supposed to be uniform and the external medium is insulating. The influence of a layer of conducting fluid at rest surrounding the experiment was examined. The magnetic field equation,

$$\partial_t \vec{B} = \nabla \times (\vec{U} \times \vec{B}) + \frac{1}{\mu\sigma}\Delta\vec{B} \qquad (1)$$

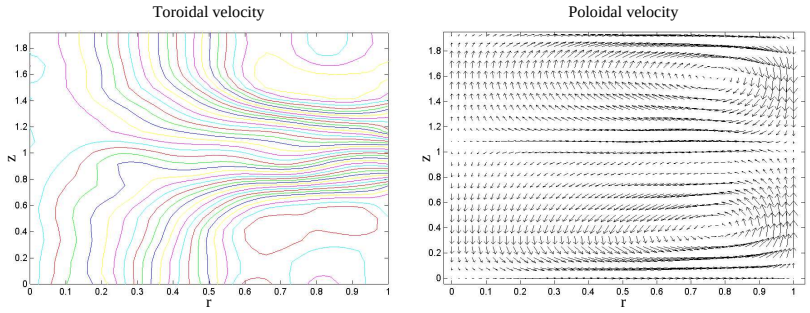

Figure 1. Mean velocity field in water experiment: (a) toroidal and (b) poloidal component of the velocity in the meridional plane. The abscissa corresponds to the normalized radius r/R, and the ordinate to the axial direction ($[0,2] \equiv$ [bottom, top]).

where $\vec{U}$ is the time averaged velocity field measured in the water prototype. It is integrated in terms of the magnetic field components:

$$\vec{B}(r,\phi,z,t) = \sum_{n,m} \vec{B}^{n,m}(r,t)\exp[i(m\phi + n\pi z)] \tag{2}$$

The energy evolution of mode (m,n),

$$E^{m,n}(t) = \frac{1}{\mu}\int_V dV |B^{m,n}(r,t)|^2 \propto e^{pt} \tag{3}$$

is recorded and self-excitation is achieved if $\mathcal{R}(p) > 0$. The results reveal an extreme sensitivity to the position of the zero of the poloidal velocity, the maximum of the toroidal velocity and the poloidal to toroidal ratio (P/T) (Burguete *et al.*, 2000). In particular, the growth rate is maximum for $P/T \simeq 0.7$ (cf. figure 2(a)).

Rm^c is also quite sensitive to the boundary condition: as shown in figure 2(b), a layer of sodium at rest of width 20% R surrounding the experiment is highly favorable. Below threshold, the study of the system response to an externally applied field exhibits a divergence of the relaxation time and of the saturation energy.

The first configuration was chosen according to the results of the optimization process: impellers that yield a poloidal to toroidal ratio ~ 0.7, an efficiency ($U_{\rm flow}/U_{\rm disc} \sim 0.9$) and copper walls ($\sigma_{\rm Cu} \sim 4\sigma_{\rm Na}$). Under these conditions the expected threshold is $Rm^c \sim 70$, for a maximum of $Rm^{\rm max} \sim 55$ with 150kW of mechanical power input. It should be emphasized that this corresponds to the dynamo action of the mean flow as if it were acting alone. No quantitative estimate of the role of the turbulent fluctuations is performed with this analysis.

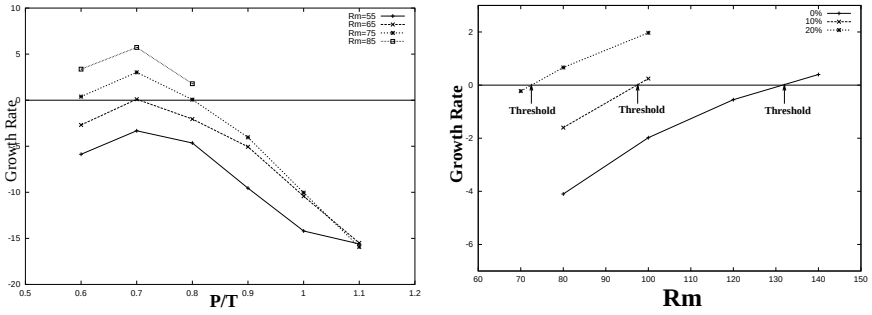

Figure 2. (a) Energy growth rate as a function of the poloidal to toroidal ratio P/T for various magnetic Reynolds numbers: $(+)$: $Rm = 55$; $(\times)$: $Rm = 65$, $(*)$: $Rm = 75$, $(\square)$: $Rm = 85$. (b) Energy growth rate as a function of the magnetic Reynolds number for various boundary condition. % indicates the proportion of sodium at rest surrounding the flow: $(+) : 0\%$, $(\times) : 10\%$, $(*) : 20\%$.

3. Experimental set-up and hydrodynamic measurements

Sodium loop : it is shown in figure 3. It is meant to be a versatile facility that can handle various flow configurations with a maximum sodium flow volume of about 300 liters. It is equiped with 2 electrical AC motors of 75kW each and a corresponding cooler is soon to be installed.

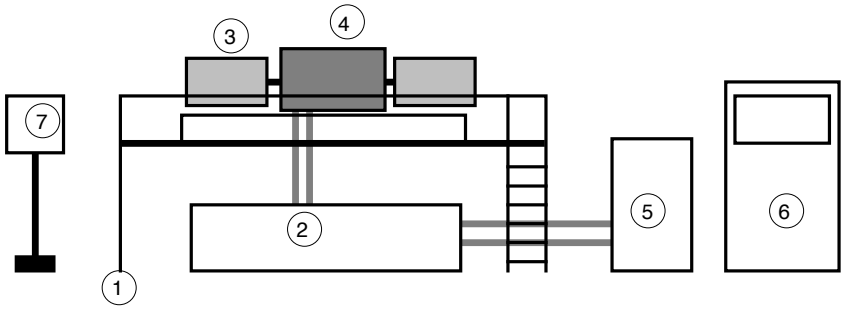

Figure 3. Sodium loop. (1) experimental platform, (2) sodium tank (270 liters), (3,4) motors and flow vessel, (5) sodium purifying unit, (6) control unit, (7) argon circuit command.

Flow : The gallium set-up has been described in details in earlier work (Odier *et al.*, 1993). The sodium flow configuration is of the same type – recalled in figure 4. The gallium experiment has a volume of about 6 litres with $2R \sim 20$ cm, insulating (steel) boundary conditions, and uses $2\times$11kW motors to drive the flow. The sodium setup holds 70 liters with $2R \sim 40$ cm, has conducting (copper shell) boundary conditions and uses $2\times$75kW motors.

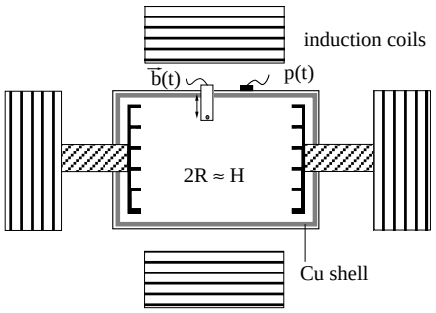

Figure 4. Experimental set-up. The magnetic induction coils can produce an applied field of about 20 Gauss inside the flow, either parallel to the rotation axis or perpendicular to it. The magnetic field is measured locally *in situ* using a Hall probe located in the median plane, at a distance $D \sim R/2$ from the rotation axis.

The rotation rates of the driving discs are equal and opposite, adjustable in the range $\Omega \in [0 - 50]$ Hz.

Both set-up are equipped with a piezoelectric pressure transducer mounted flush with the cylindrical wall. Figure 5(a) shows an example of the fluctuations in time of the pressure measured at the flow wall. The sudden drops are ascribed to concentrated vortex filaments (Fauve *et al.*, 1993; Abry *et al.*, 1994; Cadot *et al.*, 1995) that have visualized using water seeded with air bubbles (Douady *et al.*, 1991); their core size has been measured acoustically (Dernoncourt *et al.*, 1998) and is found to be of the order of the Taylor microscale. The *rms* intensity of the pressure fluctuations varies as the square of the rotation rates of the discs, as shown in figure 5(b). This yields a measurement of the intensity of the *rms* velocity fluctuations (Fauve *et al.*, 1993; Mordant *et al.*, 1997):

$$p_{rms} \sim \frac{1}{2}\rho u_{rms}^2. \tag{4}$$

This, in turn, gives an estimate of the efficiency of the discs driving the flow, evaluated as the ratio of the *rms* velocity fluctuation to the disc rim speed:

$$K_u = \frac{u_{rms}}{U_{\rm rim}} = \frac{\sqrt{2p_{rms}/\rho}}{2\pi R\Omega} \tag{5}$$

We obtain $K_u = 0.12$ for the gallium experiment using flat discs bearing an etched pattern and $K_u = 0.83$ in the sodium setup using discs with curved blades. This value is in good agreement with the optimization process and the water measurements.

For each experiment, we have also checked the scaling of the power consumption of the flow as a function of the discs rotation rate. As stated previously, a dimensional argument in the limit of very large kinetic Reynolds

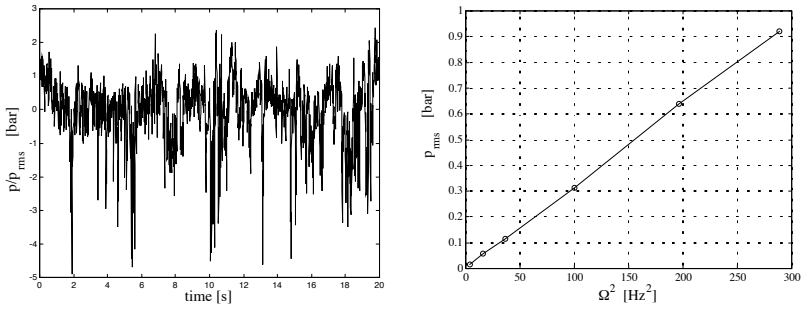

Figure 5. (a) time variation of the pressure measured at the flow wall ($\Omega = 17$ Hz); (b) evolution of the rms value of the pressure fluctuations with the discs rotation rate.

numbers yields:

$$P = K_P \, \rho R^5 \Omega^3 \quad , \tag{6}$$

where K_P is a dimensionless factor that depends on the geometry of the cell and of the shape of the driving discs. To obtain P, we monitor the current and voltage in the driving motors or we record the temperature drift inside the flow when the external cooling is turned off. Both methods give results in very good agreement. We obtain $K_P = 2.57$ in the gallium set-up (discs with a 5 mm deep etched pattern), and $K_P = 33.9$ in the sodium experiments with the discs as defined by the optimization procedure.

Magnetic measurements : Induction coils are placed with their axis either aligned with the motors rotation axis or perpendicular to it – cf. figure 4. As a result, one can apply to the flow a steady magnetic field $\vec{B}_0$ with strength in the range 1-20 Gauss. This field does not modify the flow, since the interaction parameter $N = B_0^2/\rho\mu_0 U^2$ is of the order of $N \sim 10^{-5}$. However, it is distorted by the flow motion that generates an induced field $\vec{b}$ results. We measure the three components of the local magnetic field inside the flow using a calibrated and temperature compensated 3D Hall probe (F.W. BELL). Its dynamical range is 65 dB and time resolution 20 μs. The signal is digitized using a 16-bit data acquisition card (DataTranslation) and stored on PC.

4. Results

4.1. INDUCTION

Let us begin with a description of the main characteristics of the magnetic measurements, made *in situ* and with an externally applied field. The

equation governing the magnetic field $\vec{b}$ generated by the flow, reads:

$$\partial_t \vec{b} - \frac{1}{\mu\sigma}\Delta\vec{b} = (\vec{B}_0.\vec{\nabla})\vec{u} - (\vec{u}.\vec{\nabla})\vec{b} + (\vec{b}.\vec{\nabla})\vec{u} \ . \tag{7}$$

At low Rm, the first term on the right hand side of the equation for $\vec{b}$ is dominant and the induced field is thus also proportional to Rm. At larger Rm, the two last terms of the equation for $\vec{b}$ are not negligible and the induced field is no longer proportional to Rm.

When the magnetic Reynolds number is low enough, the induction equation is dominated by the stretching term (the 'quasistatic' approximation (Golistyn, 1960; Moffatt, 1961)) and reads:

$$(\vec{B}_0.\vec{\nabla})\vec{u} + \frac{1}{\mu\sigma}\Delta\vec{b} \approx 0 \ . \tag{8}$$

For an external field $\vec{B}_0$ applied along direction $\hat{j}$, the i-th component of the induced field results from the stretching by the velocity gradient $\partial_j u_i$. At low Rm, induction is directly linked to the velocity gradient tensor $[\partial_j u_i]$; in addition, the amplitude of the induced field is directly proportional to the magnitude of the applied field (the ratio of the two provide an *intrinsic* definition of the magnetic Reynolds number – cf. (Martin *et al.*, 2000)).

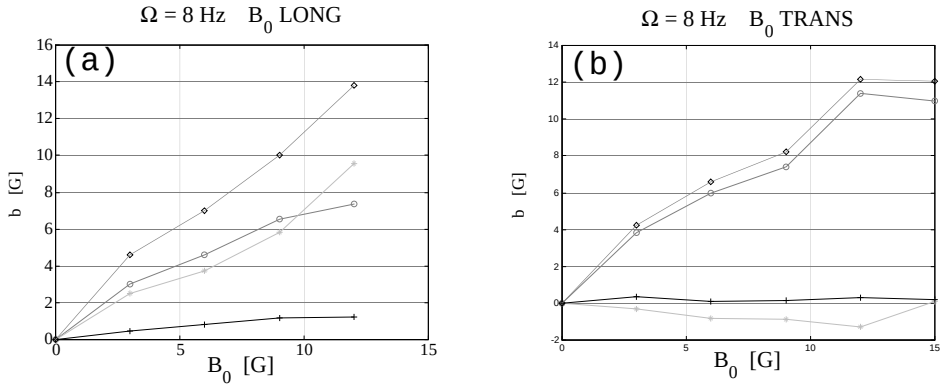

Figure 6. Induced field as a function of the applied field, for counter rotating discs at $\Omega = 8$ Hz. (a) B_0 is applied along the axis of rotation; (b) B_0 perpendicular to the axis of rotation. Symbols are: ($\circ$) axial component b_z of the induced field, ($*$) azimuthal component, ($+$) radial component and ($\diamond$) induction magnitude $||\vec{b}||$. The measurement probe is located near the mid-plane, 10 cm from the axis of rotation.

An example of the variation of the average components of the induced magnetic field with the applied field is given in figure 6. In each case, the magnitudes of the axial and azimuthal induced fields are of the same order

and both larger than that of the radial field. This is in agreement with the averaged velocity profile measurements (see figure 1. The total induced field is of the same order as the applied one:

$$\frac{\partial||\vec{b}||}{\partial B_{0,\mathrm{LONG}}} \sim 0.9 \qquad \frac{\partial||\vec{b}||}{\partial B_{0,\mathrm{TRANS}}} \sim 1.2 \ , \tag{9}$$

where $B_{0,\mathrm{LONG}}$ and $B_{0,\mathrm{TRANS}}$ are the externally applied fields along the axis of rotation or in the direction perpendicular to it (cf. figure 2).

For comparison, measurements in the gallium experiment at a comparable rotation rate gives a maximum value $\partial||\vec{b}||/\partial B_{0,\mathrm{LONG}} \sim 0.1$, while $\partial||\vec{b}||/\partial B_{0,\mathrm{TRANS}}$ is of the order of a few percent (Martin *et al.*, 2000). Recalling that this ratio is a definition of an intrinsic magnetic Reynolds number, the observed increase in induction effects when going from the gallium to the sodium experiment is attributed to the changes in the fluid electrical conductivity ($\sigma_{\mathrm{Na}} \sim 2.2\sigma_{\mathrm{Ga}}$), size of the experiment ($L_{\mathrm{Na}} \sim 2L_{\mathrm{Ga}}$) and power in the driving motors ($P_{\mathrm{Na}} \sim 7P_{\mathrm{Ga}}$). In addition, the impellers profile has been optimized for a ratio of poloidal to toroidal velocity close to 1 so that the induction have the same magnitude in the axial and transverse directions.

4.2. TIME EVOLUTION AND SPECTRUM

The data shown in the previous section are averaged over long periods of time. In fact, due to the large value of the kinetic Reynolds number of the flow, the flow is strongly turbulent, with *rms* velocity fluctuations (related to the mean) in the range 30 to 50% (see the experimental set-up section).

We show in figure 7 the time evolution of the axially induced field for a transverse B_0, at a rotation rate of $\Omega = 8$ Hz. Large fluctuations are observed with a level comparable to that of the velocity fluctuations of the flow. In addition, they occur over slow time scales: the *rms* fluctuation level is nearly unchanged if the signal is low-pass filtered below Ω or even $\Omega/10$. Such long time scales can be associated with 'global' fluctuations of the mean flow which are known to exist in this geometry (Pinton and Labbé, 1994); it is also of the order of magnitude of magnetic diffusion over the flow size ($\tau_{\mathrm{diff}} = \mu_0 \sigma R^2 \sim 1$ s). Advective time scales are much faster: for instance the advection of fluid past the Hall probe is of the order of $\tau_{\mathrm{adv}} \sim d_{\mathrm{probe}}/u_{rms} \sim (d_{\mathrm{probe}}/2\pi R)T \sim 0.024T$ ($T \equiv \Omega^{-1}$ is the integral time scale of the flow).

These time scales have a corresponding meaning in the correlation functions and power spectra of the induction field. Correlation is shown in figure 8. One observes that the autocorrelation decreases with a characteristic time of order T and is null for time lags larger than about $10T$. It shows

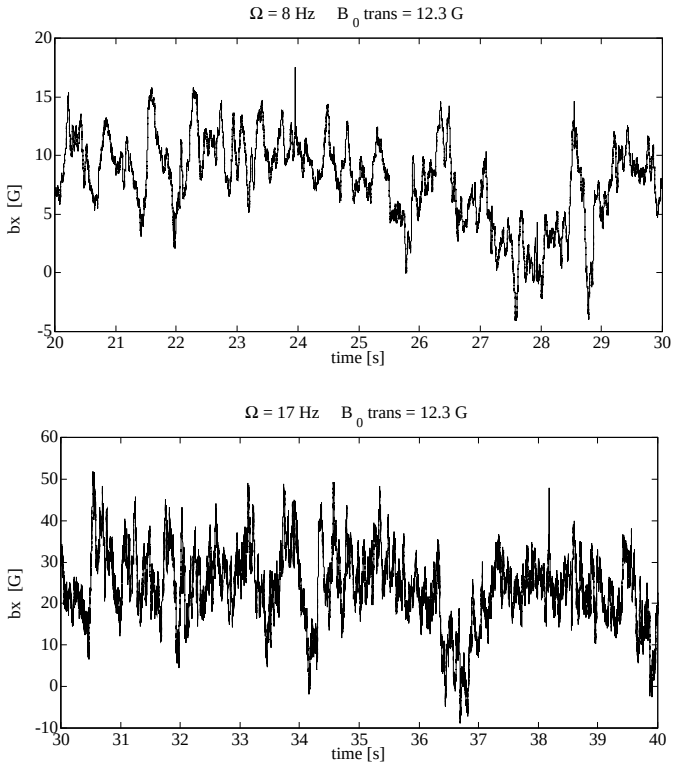

Figure 7. Time variation of the axial component of the induced field inside the flow, for a transverse applied field of magnitude $B_0 = 12.3$ G, at a rotation rate $\Omega = 8$ Hz (upper) and $\Omega = 17$ Hz (lower). The measurement probe is located near the mid-plane, 10 cm from the axis of rotation.

in particular that the drops in the induced field observed in figure 7 occur as decorrelated events. The components of the induced field are also cross-correlated (dashed lines in the main figure 8: at $\Omega = 8$ Hz, the axial and azimuthal components are correlated, whereas at $\Omega = 17$ Hz the axial and radial components are correlated. The induced field is also correlated to the pressure fluctuations (inset of figure 8):

$$\langle b(t)p(0)\rangle_{t=0} \sim \pm 0.2 \quad , \tag{10}$$

a quite significant value considering that the measurements are made at points located some 15 cm away in a flow where the Reynolds number is larger than 10^6. We thus attribute the slow variations in the magnitude of the induction to changes in the large scales of the hydrodynamic flow.

Spectra (Fourier transform of the auto correlation functions) are shown in figure 9. The curves are very similar for the three components of the induced field. Three regimes are observed: (i) for frequencies lower than

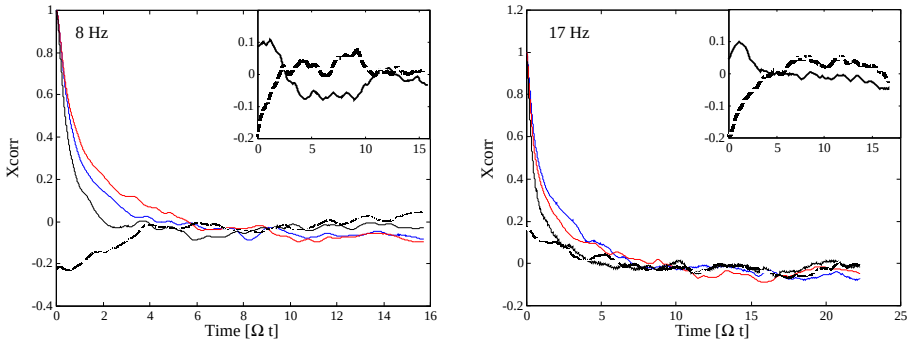

Figure 8. Correlation of induction fluctuations. Autocorrelation functions for each of the 3 components of B-field (solid line) and largest $\langle B_i B_j \rangle$ cross correlation function (dashed line). The inset shows the cross correlation function between pressure and magnetic field component (axial: solid; azimuthal: dashed). The measurement probe is located near the mid-plane, 10 cm from the axis of rotation. The pressure probe is mounted flush with the inner wall, at a distance $d = 10$ cm from the magnetic probe.

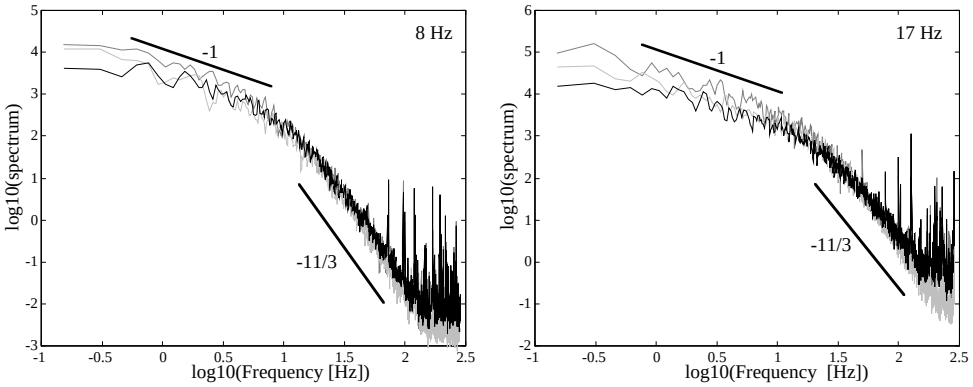

Figure 9. Power spectrum of the components of the magnetic induction. The measurement probe is located near the mid-plane, 10 cm from the axis of rotation.

about $\Omega/10$, the spectral content is flat; (ii) for frequencies between $\Omega/10$ and Ω there is a power law behavior with an exponent close to -1; (iii) for frequencies higher than Ω the spectra decay algebraically with a slope close to $-11/3$. This last regime corresponds to the turbulent fluctuations, in agreement with Kolmogorov K41 phenomenology (Moffatt, 1961), provided that a Taylor hypothesis is valid for the local field measurement. This observation is in agreement with measurements made in the Gallium experiment (Odier *et al.*, 1993). The power law regime $\tilde{b}^2(f) \propto f^{-1}$ was not readily observed in the Gallium set-up; it is consistent with measurements of the Karlsruhe experiment (Stieglitz *et al.*, 2000), and with numerical results reported in (Frisch *et al.*, 1975).

4.3. EVOLUTION WITH THE MAGNETIC REYNOLDS NUMBER

Experiments with a steady externally applied field have been made for rotation frequencies of the impellers between 0 and 24 Hz. In the case where $\vec{B}_0$ is perpendicular to the axis of rotation, the corresponding evolution of the average magnitude of the induced field $|\vec{b}|$ and of its rms fluctuations with the magnetic Reynolds number are shown in figure 10.

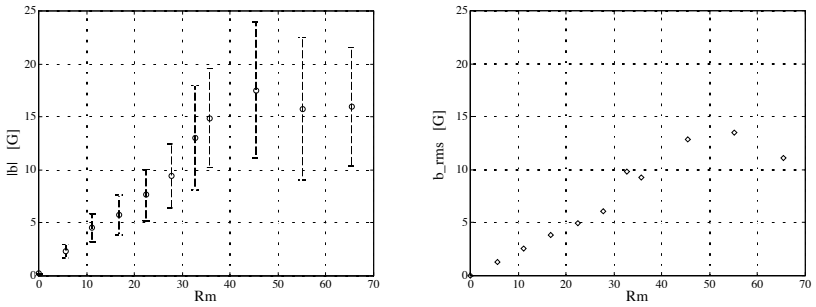

Figure 10. Induction for an applied transverse field, $B_0 = 12.3$ G. (a) Variation of the average induced magnetic field with the magnetic Reynolds number of the flow; (b) rms variation of the magnitude of $\vec{b}$ (it accounts for the error bars in (a)). In the calculation of Rm, the variations of the electrical conductivity with the sodium temperature have been accounted for. The measurement probe is located near the mid-plane, 10 cm away from the axis of rotation.

At low discs rotation speed, the behavior is linear: the induced field is proportional to the magnetic Reynolds number. As argued previously, such a linear behavior is expected at low Rm and the values of the induction strength obtained are in agreement with our optimization procedure.

At higher rotation rates, one observes a change in behavior: despite the increase in the discs rotation rate, the amplitude of the induced field saturates. As the magnitude of the induced field reaches the magnitude of the applied one, it is not surprising to observe non linear effects. For instance, when a transverse field is applied as in figure 10, an axial field component is induced (cf. figure 6(b)); this may in turn generate a transverse induced field as in figure 6(a). If this is the case in the above figure, the non-linearity tends to decrease the overall magnitude of the induced field. Further measurements are needed establish clearly these effects and their link to a possible dynamo action in this geometry.

5. Concluding remarks

A sodium experimental platform has been established in a CNRS/ENS/CEA collaboration, that has allowed new MHD measurements on von Kármán

swirling flows. The results reported here are based on the experiment first run. Further progress are expected as the experiment proceeds.

References

Abry, P. , Fauve, S., Flandrin, P. and Laroche C., *J. Phys. II France* **4**, 725-733 (1994).
Burguete J., Daviaud F., Léorat J., preprint, (2000).
Bullard E.C., *Proc. Camb. Phil. Soc*, **51**, 744-76, (1955).
Cadot, O., Douady, S. and Couder, Y., *Phys. Fluids* A**7**, 630-646 (1995).
Daviaud F., Chiffaudel A., Mari L., private communication.
Dernoncourt, B., Pinton, J. F. and Fauve, S., Physica D, **117**, 181-190, (1998).
Douady, S., Couder, Y. and Brachet, M.-E., *Phys. Rev. Lett.* **67**, 983-986 (1991).
Dudley N.L., James R.W., *Proc. Roy. Soc. Lond.*, **A425**, 407,(1989).
Fauve S., Laroche C., Castaing B., *J. Phys. II*, **3**, 271, (1993).
Frisch U., Pouquet A., Léorat J., Mazure A., *J. Fluid Mech.*, **68**, 769, (1975).
Galaitis A., Lielausis O., Dement'ev S., Placatis E., Cifersons A., Gerbeth G., Gundrum T., Stefani F., Chrsiten M., Hänel H., Will G., Phys. Rev. Lett., **84**, 4365, (2000).
Galaitis A., Lielausis O., Dement'ev S., Placatis E., Cifersons A., Gerbeth G., Gundrum T., Stefani F., Chrsiten M., Hänel H., Will G., arXiv:physics/0010047, (2000).
Golitsyn, G. S., *Sov. Phys. Dokl.*, **5**, 536-539, (1960).
Herzenberg A., Philos. Trans. Roy. Soc. London A**250**, 543 (1958).
Krause F. and Rädler K.-H., *Mean field magnetohydrodynamics and dynamo theory*, Pergamon Press (New-York, 1980).
Labbé, R., Pinton, J.-F. and Fauve, S., *Phys. Fluids*, **8**(4), 914-922, (1996).
Larmor J., *Rep. Brit. Assoc. Adv. Sci*, 159-160, (1919).
'Generation of magnetic field in the Couette-Taylor system', these proceedings.
Léorat J., Proc. Pamir Conference, Aussois(France), (1998).
Lowes F. J. and Wilkinson I., Nature **198**, 1158 (1963); **219**, 717 (1968).
Malkus W.V.R., *Science*, **60**, 259-264, (1968).
Martin A. , Odier P., Pinton J.-F., Fauve S., *Euro. J. Phys.*, to appear, (2000).
Moffatt H. K., *J. Fluid Mech.*, **11**, 625, (1961).
Moffatt H. K. , *Magnetic field generation in electrically conducting fluids*, Cambridge University Press (Cambridge 1978).
Mordant N., Pinton J.-F., Chillà F., *J. Phys. II*, **7**, 1, (1997).
Nore C., Brachet M.-E., Politano H., Pouquet A., *Phys. Plasmas*, **4**, 1, (1997).
Odier P. , Pinton J.-F., Fauve S., *Phys. Rev. E*, **58**, 7397, (1999).
Parker E. N., Astrophys. J. **122**, 293 (1955).
Peffley N.L., Cawthrone A.B., Lathrop D.P., Phys. Rev. E, **61**(5), 5287 - 5294, (2000).
Picha, K. G., *PhD Thesis, U. of Minnesota* (1957).
Picha, K. G. and Eckert, *Proc. 3rd US Natl. Cong. Appl. Mech.*, 791-798 (1958).
Pinton J.-F., Labbé R., *J. Phys.II (France)*, **4**, 1461-1468, (1994).
Ponomarenko Yu. B., J. Appl. Mech. Tech. Phys. **14**, 755 (1972).
Roberts P.H. and Jensen T. H. , Phys. Fluids B **5**, 1408 (1993) and references therein.
Roberts G. O., Phil. Trans. Roy. Soc. London A **271**, 411 (1972).
Simand C., Chillá F., Pinton J.-F., in "Vortex structure and dynamics",, 285-292, LNP555, Spinger, (2000).
Stieglitz R., Müller U., Naturwissenschaften, **87**(9), 381-390, (2000).
Welsh, W. E. and Harnett, J. P., *Proc. 3rd US Nat. Cong. Appl. Mech.* (1958).
Zandbergen P. J., Dijkstra D., *Ann. Rev. Fluid Mech.*, **19**, 465, (1987).